



Balancing the Power-to-Load Ratio for a Novel Variable Geometry Wave Energy Converter with Nonideal Power Take-Off in Regular Waves

Preprint

Nathan Tom, Yi-Hsiang Yu, and Alan Wright
National Renewable Energy Laboratory

*Presented at the European Wave and Tidal Energy Conference
Cork, Ireland*

August 27–September 2, 2017

**NREL is a national laboratory of the U.S. Department of Energy
Office of Energy Efficiency & Renewable Energy
Operated by the Alliance for Sustainable Energy, LLC**

This report is available at no cost from the National Renewable Energy Laboratory (NREL) at www.nrel.gov/publications.

Conference Paper
NREL/CP-5000-68082
September 2017

Contract No. DE-AC36-08GO28308

NOTICE

The submitted manuscript has been offered by an employee of the Alliance for Sustainable Energy, LLC (Alliance), a contractor of the US Government under Contract No. DE-AC36-08GO28308. Accordingly, the US Government and Alliance retain a nonexclusive royalty-free license to publish or reproduce the published form of this contribution, or allow others to do so, for US Government purposes.

This report was prepared as an account of work sponsored by an agency of the United States government. Neither the United States government nor any agency thereof, nor any of their employees, makes any warranty, express or implied, or assumes any legal liability or responsibility for the accuracy, completeness, or usefulness of any information, apparatus, product, or process disclosed, or represents that its use would not infringe privately owned rights. Reference herein to any specific commercial product, process, or service by trade name, trademark, manufacturer, or otherwise does not necessarily constitute or imply its endorsement, recommendation, or favoring by the United States government or any agency thereof. The views and opinions of authors expressed herein do not necessarily state or reflect those of the United States government or any agency thereof.

This report is available at no cost from the National Renewable Energy Laboratory (NREL) at www.nrel.gov/publications.

Available electronically at SciTech Connect <http://www.osti.gov/scitech>

Available for a processing fee to U.S. Department of Energy and its contractors, in paper, from:

U.S. Department of Energy
Office of Scientific and Technical Information
P.O. Box 62
Oak Ridge, TN 37831-0062
OSTI <http://www.osti.gov>
Phone: 865.576.8401
Fax: 865.576.5728
Email: reports@osti.gov

Available for sale to the public, in paper, from:

U.S. Department of Commerce
National Technical Information Service
5301 Shawnee Road
Alexandria, VA 22312
NTIS <http://www.ntis.gov>
Phone: 800.553.6847 or 703.605.6000
Fax: 703.605.6900
Email: orders@ntis.gov

Cover Photos by Dennis Schroeder: (left to right) NREL 26173, NREL 18302, NREL 19758, NREL 29642, NREL 19795.

NREL prints on paper that contains recycled content.

Balancing the Power-to-Load Ratio for a Novel Variable Geometry Wave Energy Converter with Nonideal Power Take-Off in Regular Waves

Nathan Tom

National Renewable Energy Laboratory
15013 Denver West Parkway
Golden, CO 80401, USA
E-mail: Nathan.Tom@nrel.gov

Yi-Hsiang Yu

National Renewable Energy Laboratory
15013 Denver West Parkway
Golden, CO 80401, USA
E-mail: Yi-Hsiang.Yu@nrel.gov

Alan Wright

National Renewable Energy Laboratory
15013 Denver West Parkway
Golden, CO 80401, USA
E-mail: Alan.Wright@nrel.gov

Abstract—This work attempts to balance power absorption against structural loading for a novel variable geometry wave energy converter. The variable geometry consists of four identical flaps that will be opened in ascending order starting with the flap closest to the seafloor and moving to the free surface. The influence of a pitch motion constraint on power absorption when utilizing a nonideal power take-off (PTO) is examined and found to reduce the losses associated with bidirectional energy flow. The power-to-load ratio is evaluated using pseudo-spectral control to determine the optimum PTO torque based on a multiterm objective function. The pseudo-spectral optimal control problem is extended to include load metrics in the objective function, which may now consist of competing terms. Separate penalty weights are attached to the surge-foundation force and PTO control torque to tune the optimizer performance to emphasize either power absorption or load shedding. PTO efficiency is not included in the objective function, but the penalty weights are utilized to limit the force and torque amplitudes, thereby reducing losses associated with bidirectional energy flow. Results from pseudo-spectral control demonstrate that shedding a portion of the available wave energy can provide greater reductions in structural loads and reactive power.

Index Terms—Pseudo-Spectral Control, Variable Geometry, Load Shedding, PTO Efficiency, Wave Energy Converter

I. INTRODUCTION

At the 11th European Wave and Tidal Energy Conference (EWTEC), a fixed-bottom oscillating surge wave energy converter (OSWEC) [1], [2] was introduced that replaced the main body with control flaps [3]. The control surfaces allow for a variable geometry device that can alter its hydrodynamic characteristics to favor either power absorption or load shedding. The variable geometry concept has been shown to be successful at mitigating loads, especially fatigue damage accumulation, in moderate-to-large sea states [4], [5]. In previous studies [4], [5], the variable geometry flaps were opened in descending order starting with the flap positioned closest to the free surface; however, the reduction in hydrodynamic coefficients has been deemed too large, prompting this investigation to reverse the order in which the flaps are opened. It is desired to combine manipulation of the variable geometry components with power-take-off (PTO) control in an

attempt to control peak loads rather than focus on power maximization [6]. Wave energy converter (WEC) control strategies, such as complex conjugate [7] and latching [8], continue to receive attention from the marine engineering community, but emphasis is still predominately placed on maximizing energy capture. However, if control emphasis is placed solely on power maximization, the structural and PTO loads may greatly exceed the growth in absorbed energy. Therefore, it will be of value to begin developing control strategies that attempt to increase power absorption while minimizing peak forces [9], torques [6], [10], and fatigue damage accumulation [11].

The appeal of state-constrained optimization [12] has continued to gain popularity in recent years as a result of increases in computational power. This type of optimization has most recently been demonstrated using model predictive control [9], [13] and pseudo-spectral methods [14], [15]. One simplification that is often used in WEC control is an perfectly efficient PTO unit, which can be a poor assumption if bidirectional energy flow is allowed. Other investigations have attempted to represent the PTO efficiency directly in the objective function of the optimizer [16], [17]; however, these methods result in a nonlinear objective function that increases the solution complexity and computational time. In contrast, this investigation will rely on the use of penalty weights applied to the load metrics to control the additional losses resulting from use of a nonideal PTO. Therefore, no direct measure of PTO efficiency is included in the objective function, but it is expected that reducing the structural and PTO loads will limit the negative peaks in instantaneous power that result in greater nonlinear effects on the time-averaged power (TAP).

This paper begins with a review of the variable geometry OSWEC and presents the radiation and excitation hydrodynamic coefficients for the geometries used in this study. The analysis will be completed under regular wave excitation with a constraint set on the pitch angular displacement, which reduces the upper limit on the maximum power capture. In order to absorb the maximum power available, it is necessary that the PTO use both a linear damping and spring component;

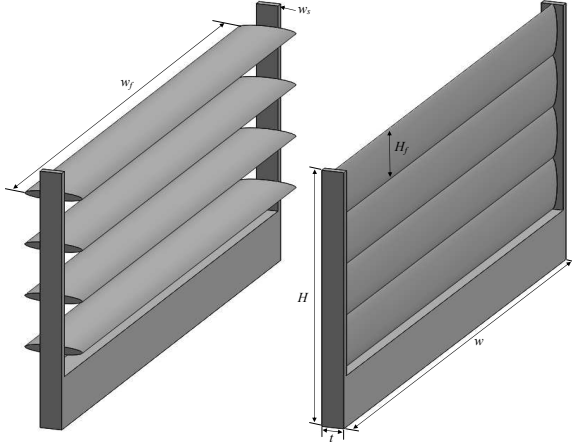


Fig. 1. Solidworks rendering of the novel OSWEC. Perspective view of the fully open configuration (left, four flaps open) and perspective view of the fully closed configuration (right, zero flaps open).

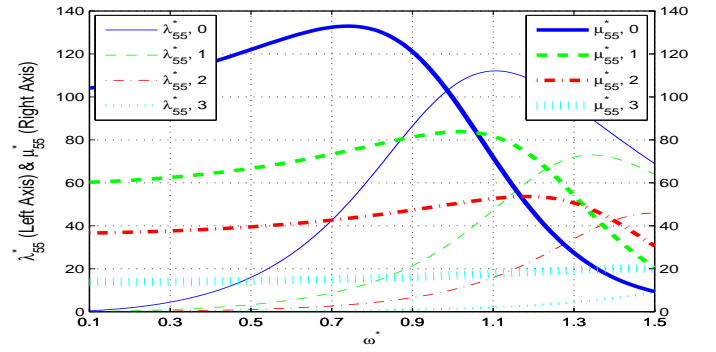
TABLE I
GEOMETRIC AND MASS PARAMETERS OF THE OSWEC

Water Depth, h , 10 m	Flap Minor Axis, t_f , 1/3 m
Height, H , 10 m	Flap Major Axis, H_f , 2 m
Thickness, t , 3/4 m	Side Support Width, w_s , 1/4 m
Width, w , 20 m	Center of Gravity, r_g , 3.97 m
Flap Width, w_f , 19.5 m	Moment of Inertia, I_{55} , 904.4 kg-m ²
Volume, ∇ , 72 m ³	Mass, m , 36 t
Resonance Period, T_{res}	Resonance Frequency, ω_{res}
Zero-Open Flap, 51.84 s	Zero-Open Flap, 0.10 rad/s
One-Open Flap, 39.62 s	One-Open Flap, 0.16 rad/s
Two-Open Flap, 31.10 s	Two-Open Flap, 0.20 rad/s
Three-Open Flap, 19.49 s	Three-Open Flap, 0.32 rad/s

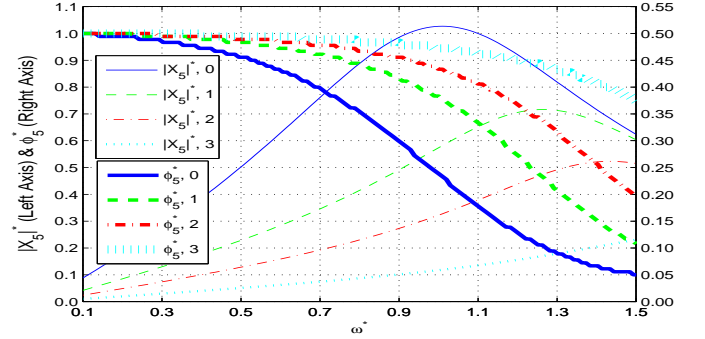
however, having a nonzero PTO spring coefficient guarantees bi-directional energy flow. The reversal of the energy flow will generate additional losses, and calculation of the TAP delivered to the grid from a nonideal PTO is therefore introduced. Next, the theory of pseudo-spectral control is reviewed, which includes the incorporation of the surge-foundation force and PTO control torque in the objective function. The effect of the penalty weights, associated with each load contribution, on optimizer performance was observed by varying the magnitudes of each across a range of wave periods and several wave amplitudes.

II. OSWEC HYDRODYNAMIC MODELING

As described in previous studies [4], [5], the main body of the novel OSWEC has been replaced with a set of identical flaps that may rotate about its center axis (see Fig. 1). The actuated flaps can be adjusted to any desired angle about their center of rotation; however, for this investigation, the flaps were placed in either the fully closed or open configurations. The flaps may be opened independently, but will only be allowed to open in ascending order starting with the bottom flap located closest to the seabed. Therefore, no geometry is modeled that consists of a closed flap between two open flaps. Previously, the flaps were opened in descending order starting with the flap closest to the free surface. However, the changes



(a) Radiation Pitch-Wave Damping λ_{55}^* and Added Moment of Inertia μ_{55}^*



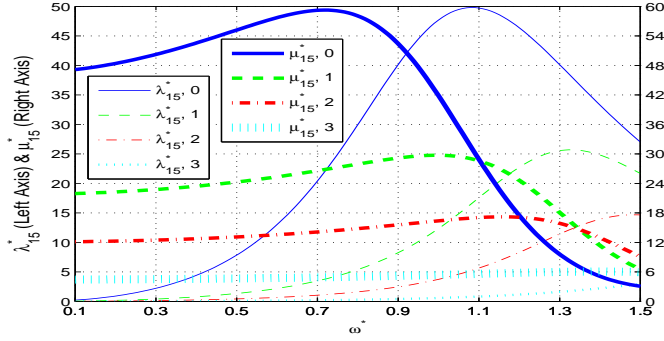
(b) Pitch-Wave Exciting Torque Magnitude $|X_5^*|$ and Phase ϕ_5^*

Fig. 2. Nondimensional hydrodynamic pitch radiation and pitch-wave excitation torque coefficients. The numbers in the legend correspond to the zero-flap, one-flap, two-flap, and three-flap geometry. The nondimensionalization is given by: $\omega^* = \omega\sqrt{h/g}$, $\mu_{55}^* = \mu_{55}/I_{55}$, $\lambda_{55}^* = \lambda_{55}/\omega I_{55}$, $X_5^* = X_5/\rho gh^2 w$, $\phi_i^* = \phi_i/\pi$.

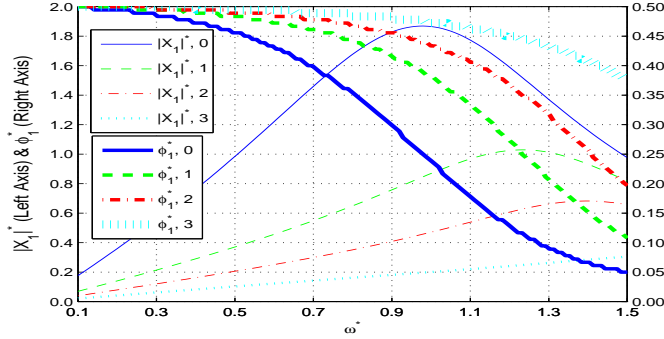
to the hydrodynamic properties with each open flap were found to be too large for smooth power production in greater sea states. The primary dimensions and mass characteristics can be found in Table I. A water depth of 10 m was chosen after reviewing previous works on fixed-bottom OSWEC systems [1], [20].

The structural mass is assumed to be evenly distributed and the structural mass density, ρ_m , was set to half the fluid density, ρ . The hydrodynamic coefficients were obtained from WAMIT version 7.2 [18] at a step size of 0.01 rad/s for wave frequencies between 0 rad/s and 7.5 rad/s with the pitch radiation added moment of inertia and wave damping coefficients plotted in Fig. 2(a), while the pitch wave excitation torque magnitude and phase are plotted in Fig. 2(b). The surge-pitch hydrodynamic coefficients plotted in Fig. 3 are used to calculate the structural foundation forces that will be outlined in Section III-B.

As shown in Fig. 2, the variable-geometry OSWEC makes it possible to control the hydrodynamic coefficients based on the number of open flaps. As each flap is opened, the radiation added moment of inertia decreases and, because the hydrostatic restoring coefficient and mass moment of inertia remain constant, the pitch resonance frequency will shift to a lower period (higher frequency). However, the reduction in the hydrodynamic coefficients is not uniform when opening an



(a) Radiation Surge-Pitch Wave Damping (λ_{15}^*) and Added Inertia (μ_{15}^*)



(b) Surge-Wave Exciting Force Magnitude ($|X_1^*|$) and Phase (ϕ_1^*)

Fig. 3. Nondimensional hydrodynamic surge-pitch radiation and surge-wave exciting force coefficients. The numbers in the legend correspond to the zero-flap, one-flap, two-flap, and three-flap geometry. The nondimensionalization is: $\mu_{15}^* = \mu_{15}/mh$, $\lambda_{15}^* = \lambda_{15}/\omega mh$, $X_1^* = X_1/\rho g wh$, $\phi_i^* = \phi_i/\pi$.

additional flap, with the largest decrease occurring between the zero- and one-flap open geometries. These results have prompted an investigation into the use of nonuniform flap heights [19] to provide a more gradual reduction in the hydrodynamic coefficients. Although the peak values for the hydrodynamics decrease with each additional open flap, the wave frequency at which a given quantity is maximized shifts to shorter wave periods similar to previous investigations.

III. REGULAR WAVE ANALYSIS

This analysis assumes regular wave excitation with the incident wave elevation described by

$$\eta(x, t) = A \cos(\omega t - kx) \quad (1)$$

where η is the wave elevation, A is the wave amplitude, ω is the wave angular frequency, and k is the wave number. For the time being, the mechanical torque from the PTO system will be described by

$$\tau_m(t) = -\Re \{ (\lambda_g - iC_g/\omega) i\omega \xi_5 e^{i\omega t} \} \quad (2)$$

where C_g is the linear PTO-restoring coefficient, λ_g is the PTO linear-damping coefficient, and ξ_5 is the complex amplitude of the pitch angular displacement. The frequency-domain expressions can be inserted into the one-degree-of-freedom

pitch equation of motion to derive the pitch-angular-velocity response amplitude operator (RAO):

$$\frac{i\omega \xi_5}{A} = \frac{X_5}{[\lambda_{55} + \lambda_g] + i[-(C_{55} + C_g)/\omega + \omega(I_{55} + \mu_{55})]} \quad (3)$$

$$\frac{\alpha_m}{A} = \frac{[C_g + i\omega \lambda_g] X_5}{[C_{55} + C_g + \omega^2(I_{55} + \mu_{55})] + i\omega[\lambda_{55} + \lambda_g]} \quad (4)$$

where C_{55} is the linearized hydrostatic spring constant, I_{55} is the mass moment of inertia, and α_m is the complex PTO torque amplitude. The maximum TAP [21], per wave amplitude squared, absorbed by an ideal PTO unit can be calculated from

$$\begin{aligned} \frac{P_T}{A^2} &= \frac{1}{4} \frac{|X_5|^2}{\lambda_{55}} \frac{1}{1 + \sqrt{1 + \left(\frac{C_{55} + C_g - \omega^2(I_{55} + \mu_{55})}{\omega \lambda_{55}} \right)^2}} \\ &= \frac{2\rho g V_g}{k} \frac{1}{1 + \sqrt{1 + \left(\frac{C_{55} + C_g - \omega^2(I_{55} + \mu_{55})}{\omega \lambda_{55}} \right)^2}} \quad (5) \end{aligned}$$

$$\lambda_g = \lambda_{55} \sqrt{1 + \left(\frac{C_{55} + C_g - \omega^2(I_{55} + \mu_{55})}{\omega \lambda_{55}} \right)^2} \quad (6)$$

where V_g is the wave group velocity and the Haskind relation [22] has been used in Eqn. (5). As seen in Fig. 4, the first term in Eqn. (5) is constant for each geometry while Ξ will vary between 0-0.5. The value of Ξ will reach 0.5 when the device oscillates at the resonance frequency and can reach a similar value when the contribution from the wave damping greatly exceeds the sum of the spring and inertial terms. Both cases can be observed in Fig. 4. The first occurs when the three-flap geometry oscillates at resonance (0.32 rad/s) and the second occurs in the high-frequency range ($\omega > 1.1$ rad/s). Refer to Fig. 2(a) to observe how, for the zero- and one-flap geometries, the added moment of inertia has a steep decline while the wave damping reaches its peak. It is observed that the zero-flap geometry can theoretically absorb the greatest amount of power passively ($C_g = 0$) over the widest range of wave frequencies following the arguments made in [23]; however, this explains only half of the problem, as the required structural loads have not yet been considered.

The instantaneous power absorbed by an ideal power-take-off unit [24] can be calculated from

$$P(t) = \frac{\lambda_g |i\omega \xi_5|^2}{2} + \frac{|i\omega \xi_5|^2}{2} |Z| \cos(2(\omega t + \varphi) + \nu) \quad (7)$$

where $Z = \lambda_g - iC_g/\omega$, ν is the phase angle of Z , and φ is the phase angle of $i\omega \xi_5$. As seen from (7), if $C_g \neq 0$, the instantaneous power will fluctuate between negative and positive values, indicating a reversal of the energy flow. The time-averaged reactive power, defined as the power that the PTO returns to the oscillating body, is then calculated from

$$P_R = \frac{1}{T} \int_0^T \min[P(t), 0] dt \quad (8)$$

To provide a measure of the capture efficiency for a given WEC, the TAP contained within a propagating wave must

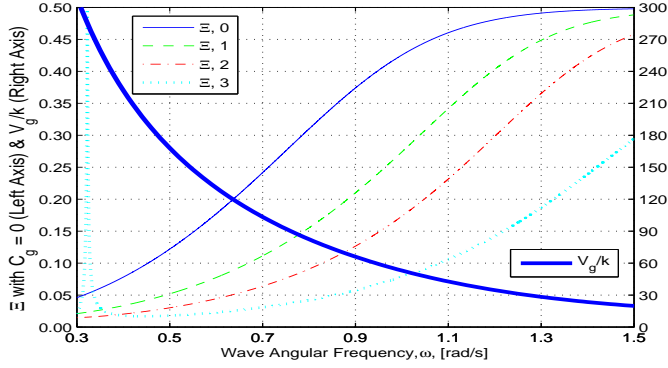


Fig. 4. The variation of Ξ ($C_g = 0$) and V_g/k with ω for each flap configuration. The numbers in the legend correspond to the zero-flap, one-flap, two-flap, and three-flap geometry.

be known. The time-averaged wave-power-per-unit width, P_w , can be calculated from

$$P_w = \frac{1}{4} \rho g A^2 \sqrt{\frac{g}{k} \tanh kh} \left[1 + \frac{2kh}{\sinh 2kh} \right] \quad (9)$$

where h is the water depth. The nondimensional capture width, C_w , in this work will be defined as

$$C_w = \frac{P_T}{w P_w} \quad (10)$$

where w is the width of the OSWEC.

A. Maximum PTO Absorbed Power under Motion Constraints

The maximum power absorption under pitch amplitude constraints, while assuming sinusoidal motion, was explored in [25], which provided the following expression

$$P_T = \begin{cases} \frac{1}{8} A^2 |X_5|^2 / \lambda_{55} & , \delta > 1 \\ \frac{1}{2} A |X_5| \omega |\xi_5|_{max} - \lambda_{55} \omega^2 |\xi_5|_{max}^2 & , \delta < 1 \end{cases} \quad (11)$$

where δ is the ratio between the constrained-to-optimal pitch-angular velocity given by

$$\delta = \frac{\omega |\xi_5|_{max} 2\lambda_{55}}{A |X_5|} \quad (12)$$

To achieve the power output described above, the associated PTO coefficients are given by

$$\lambda_g = \begin{cases} \lambda_{55} & , \delta > 1 \\ \frac{A |X_5|}{\omega |\xi_5|_{max}} - \lambda_{55} & , \delta < 1 \end{cases} \quad (13)$$

$$C_g = - [C_{55} - \omega^2 (I_{55} + \mu_{55})] \quad (14)$$

where the PTO spring coefficient must combine to cancel the torque contribution from the natural body-restoring coefficient, mass moment of inertia, and hydrodynamic added moment of inertia, which is the basis of complex conjugate control [7].

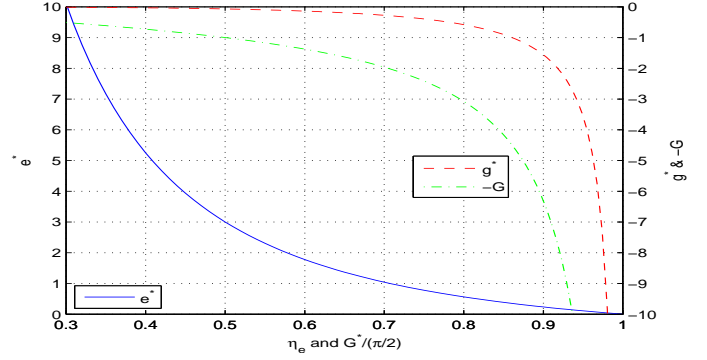


Fig. 5. The effect on e^* and g^* for a range of η_e and G values.

1) *Nonideal PTO Units:* As discussed in [26] and [27], reactive control requires a two-way energy flow between the oscillating body and an energy storage system that will have losses associated with the energy-flux reversal process. These losses will be subtracted from the power input to the PTO whenever $P(t) > 0$, and added when $P(t) < 0$ to supply power to the wave energy converter. Considering a nonideal PTO unit, with a mechanical-to-electrical efficiency defined by η_e , the resulting PTO output TAP is given by [27]

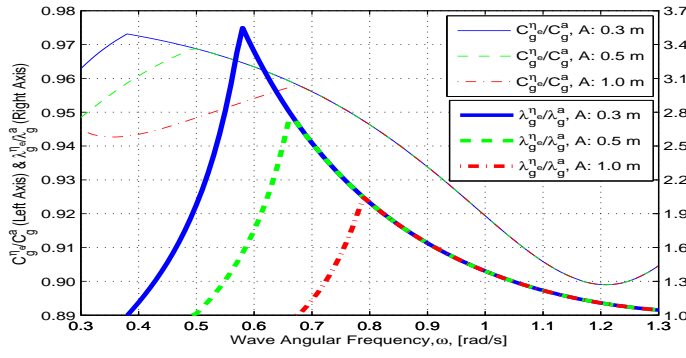
$$P_O = \eta_e \frac{\lambda_g |i\omega \xi_5|^2}{2} \{1 + e^* g^*\} \quad (15)$$

$$g^* = \frac{2G^* - \sin 2G^* - 2G(1 - \cos^2 G^*)}{2\pi} \quad (16)$$

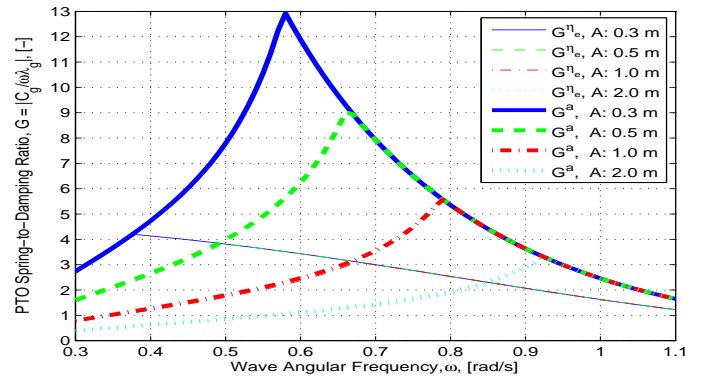
$$G = \left| \frac{C_g}{\omega \lambda_g} \right| \quad , \quad G^* = \arctan G \quad , \quad e^* = \frac{1 - \eta_e^2}{\eta_e^2} \quad (17)$$

where P_O is the time-averaged power that is sent to the grid. The variation in the terms e^* and g^* with respect to the PTO coefficients has been plotted in Fig. 5. The effect of the nonideal efficiency on the selection of the PTO coefficients (C_g & λ_g) to maximize the PTO absorbed power and the PTO output power has been plotted in Fig. 6. As plotted in Fig. 6(a), the PTO spring coefficient decreases by up to 10% at the highest wave frequencies when accounting for the PTO efficiency while the damping coefficient can increase by over 300% when at the lowest wave amplitude. However, the ratio of the PTO damping coefficient is equal to one when the motion amplitude required to maximize the output power hits the pitch-displacement amplitude constraint (refer to Fig. 6(c)), in addition to greater detuning of the response by decreasing the spring coefficient. In this range, the results from maximizing the output power will be almost identical to maximizing the absorbed power as shown in Fig. 6(b). To understand why the pitch-amplitude constraint is affecting the selection of the PTO coefficients as previously described, begin by inserting the expression for the PTO damping coefficient (when $\delta < 1$), Eqn. (13), into the expression for G

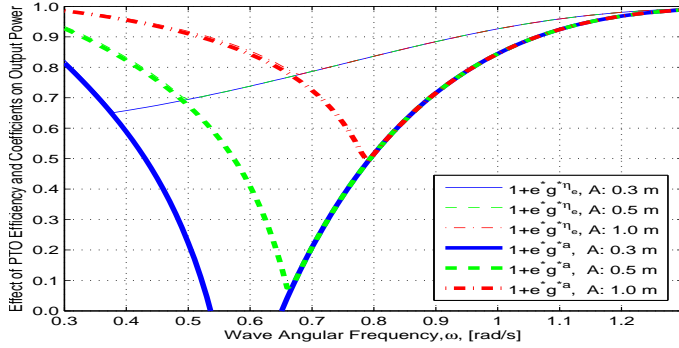
$$G = \left| \frac{C_{55} - \omega^2 (I_{55} + \mu_{55})}{\omega \left(\frac{A |X_5|}{\omega |\xi_5|_{max}} - \lambda_{55} \right)} \right| = \left| \frac{C_{55} - \omega^2 (I_{55} + \mu_{55})}{A \left(1 - \frac{\delta}{2} \right) \frac{|X_5|}{|\xi_5|_{max}}} \right| \quad (18)$$



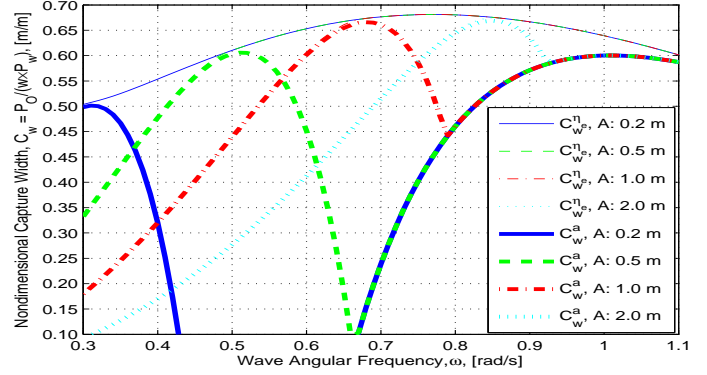
(a) Ratios of the Spring and Damping Coefficients That Will Maximize the PTO Absorbed or PTO Output Power Sent to the Grid



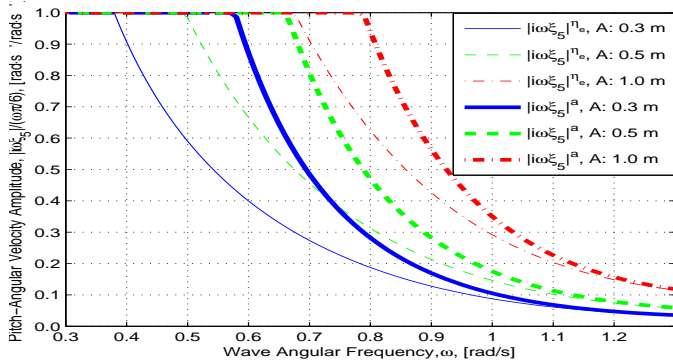
(a) PTO Spring-to-Damping Ratio, G



(b) Value of the Corrective Term, $1 + e^* g^*$, Resulting from a Nonideal PTO



(b) Nondimensional Output Capture Width, $C_w = P_O / (w \times P_w)$



(c) Pitch-Angular Velocity Amplitude $|i\omega \xi_5|$

Fig. 6. The presented results are for the one-flap-open geometry with a PTO efficiency of 85%. The superscript a denotes the performance achieved by maximizing the PTO absorbed power as shown in Eqns. (11)-(14). The superscript η_e denotes the performance achieved by maximizing the PTO output power as described in Eqns. (15)-(17).

where in the above expression, as the wave amplitude increases all terms are constant except for A and δ . However, as A increases δ decreases, which provides a nonlinear increase in the denominator. As shown in Fig. 7(a), the peak in G for an A of 0.3 m is 13, but after increasing the A to 2 m, the value of G drops to 1 leading to a greater reduction in G compared to the increase in wave amplitude. As a result, the curves for the nondimensional capture width between the maximum output and absorbed have nearly converged when oscillating with the 2-m wave amplitude (see Fig. 7(b)).

Fig. 7. The results presented are for the one-flap-open geometry with a PTO efficiency of 85%. The superscript a denotes the performance achieved by maximizing the PTO absorbed power as shown in Eqns. (11)-(14). The superscript η_e denotes the performance achieved by maximizing the PTO output power as described in Eqns. (15)-(17).

B. Structural Foundation Forces

The structural foundation must handle the reaction forces needed to anchor the WEC to the seabed. If centrifugal forces are neglected and the body remains symmetric about the vertical plane, the foundation forces in the surge, X_{r1} , and heave, X_{r3} , directions are given by [28]

$$A(X_{r1} + X_1) = [\lambda_{15} + i\omega\mu_{15}]i\omega\xi_5 \quad (19)$$

$$A(X_{r3} + X_3) + (\rho\nabla - m)g = 0 \quad (20)$$

where X_1 and X_3 are the complex surge and heave wave-exciting force coefficients per unit wave amplitude, μ_{15} is the surge-pitch added mass, and λ_{15} is the surge-pitch wave radiation damping. The following analysis does not include the heave foundation force in the final results because this force is unaffected by the WEC motion and cannot be controlled by the PTO. The surge-foundation force can theoretically be eliminated if the complex pitch-angular velocity amplitude and PTO control-torque amplitude are equal to

$$\frac{i\omega\xi_5}{A} = \frac{X_1}{\lambda_{15} + i\omega\mu_{15}} \quad (21)$$

$$\frac{\tau_m}{A} = \frac{\lambda_{55} + i[-C_{55}/\omega + \omega(I_{55} + \mu_{55})]}{\lambda_{15} + i\omega\mu_{15}} X_1 - X_5 \quad (22)$$

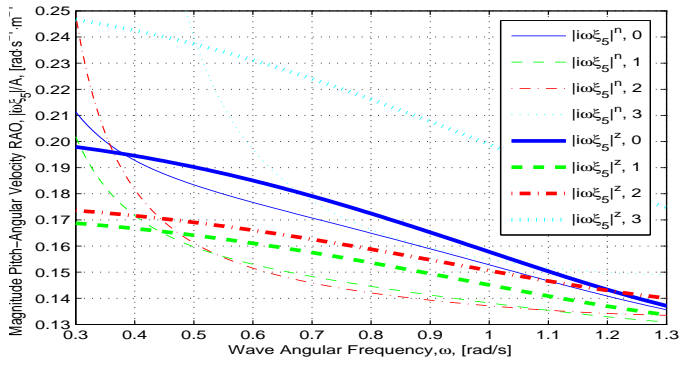


Fig. 8. Magnitude of the pitch-angular-velocity response amplitude operator for varying wave angular frequency. The superscript n denotes the natural body dynamics ($C_g = \lambda_g = 0$) obtained from solving the pitch equation of motion. The superscript z denotes the pitch dynamics required to eliminate the surge foundation force as given by Eqn. (21).

The magnitude of the pitch-angular velocity required to eliminate the surge-foundation force has been plotted in Fig. 8. This plot shows that for the OSWEC design, the natural body motion is close to the dynamics needed for elimination of the surge-foundation force, as the pitch magnitude and phase are closely aligned. The wave frequency range plotted in Fig. 8 is above the resonance frequency of each flap geometry; however, for frequencies below resonance, this is not the case because the phase of pitch motion can shift by π and the required pitch velocity amplitude may increase [10]. When the WEC begins to absorb power from the incident waves, the magnitude and phase of the pitch motion will lead to an increase in the surge-foundation force. As both the magnitude and phase of WEC motion contribute to the surge-foundation force, it may be possible to control the pitch dynamics to obtain a greater rate of growth in power than structural loading [6] and [10].

IV. REVIEW OF PSEUDO-SPECTRAL CONTROL

The pitch-angular velocity, $\dot{\zeta}_5$, and PTO control torque, τ_m , are approximated by a zero-mean truncated Fourier series [29] with N terms

$$\dot{\zeta}_5(t) \approx \sum_{j=1}^{N/2} \psi_j^c \cos(j\omega_0 t) + \psi_j^s \sin(j\omega_0 t) = \Phi(t) \hat{\psi} \quad (23)$$

$$\tau_m(t) \approx \sum_{j=1}^{N/2} \tau_j^c \cos(j\omega_0 t) + \tau_j^s \sin(j\omega_0 t) = \Phi(t) \hat{\tau} \quad (24)$$

where

$$\hat{\psi} = [\psi_1^c, \psi_1^s, \dots, \psi_{N/2}^c, \psi_{N/2}^s]^\top \quad \hat{\tau} = [\tau_1^c, \tau_1^s, \dots, \tau_{N/2}^c, \tau_{N/2}^s]^\top \quad (25)$$

$$\Phi(t) = [\cos \omega_0 t, \sin \omega_0 t, \dots, \cos(N/2)\omega_0 t, \sin(N/2)\omega_0 t]$$

with the fundamental frequency given by $\omega_0 = 2\pi/T$ and T being the chosen time duration. It can be shown that the pitch equation of motion can be described as follows

$$M_{55} \hat{\psi} = \hat{\tau} + \hat{e}_5 \quad (26)$$

where \hat{e}_5 represents the Fourier coefficients of the pitch-wave-exciting torque. The matrix $M_{55} \in \mathbf{R}^{N \times N}$ is block diagonal with the following structure

$$M_{55}^j = \begin{bmatrix} \beta(j\omega_0) & \alpha(j\omega_0) \\ -\alpha(j\omega_0) & \beta(j\omega_0) \end{bmatrix}, \quad \text{for } j = 1, 2, \dots, N/2$$

$$\alpha(j\omega_0) = j\omega_0 (I_{55} + \mu_{55}(j\omega_0)) - C_{55}/(j\omega_0)$$

$$\beta(j\omega_0) = \lambda_{55}(j\omega_0) \quad (27)$$

The pitch-angular-velocity coefficients can then be determined explicitly from the control and pitch-wave-exciting torque Fourier coefficients. This representation allows the time-averaged absorbed power, P_T , to be written as

$$P_T = \frac{1}{2} \hat{\psi}^\top \hat{\tau} = \frac{1}{2} \left[\hat{\tau}^\top (M_{55}^{-1})^\top \hat{\tau} + \hat{e}_5^\top (M_{55}^{-1})^\top \hat{\tau} \right] \quad (28)$$

which is in the form of a traditional quadratic problem. This representation does not account for nonunity efficiency; however, from this point forward any results from pseudo-spectral control will make corrections for PTO efficiency in postprocessing.

A. Surge-Foundation-Force Penalty Term

The surge-foundation force can be written in a matrix form, similar to Eqn. (26), as follows

$$\hat{f}_{r1} = -\hat{e}_1 + G_{15} \hat{\psi} = -\hat{e}_1 + G_{15} M_{55}^{-1} \hat{\tau} + G_{15} M_{55}^{-1} \hat{e}_5 \quad (29)$$

where \hat{e}_1 represents the Fourier coefficients of the surge wave-exciting force, G_{15} and Γ are block matrices (see [6] for definition), and Eqn. (26) has been substituted for $\hat{\psi}$. To maintain the convexity of the quadratic problem, the time-averaged ℓ^2 -norm of the surge-foundation-force vector was added to the objective function and is given by

$$\frac{\gamma}{2} \hat{f}_{r1}^\top \hat{f}_{r1} \approx \frac{\gamma}{2} \left(\hat{\tau}^\top (M_{55}^{-1})^\top G_{15}^\top G_{15} M_{55}^{-1} \hat{\tau} + 2 [-\hat{e}_1^\top G_{15} M_{55}^{-1} + \hat{e}_5^\top (M_{55}^{-1})^\top G_{15}^\top G_{15} M_{55}^{-1}] \hat{\tau} \right) \quad (30)$$

where γ is a penalty weight that can be used to adapt the controller performance. In the final expression for the surge-foundation-force contribution, there are three constant terms, independent of the control torque, which are left out of the optimization.

B. Control-Torque-Magnitude Penalty Term

In an attempt to reduce the reactive power contribution and limit the PTO torque amplitudes, a penalty weight was placed on the time-averaged ℓ^2 -norm of the PTO torque magnitude [9] as follows

$$\frac{\beta_m}{T} |\tau_m|^2 = \frac{\beta_m}{T} \int_0^T \tau_m(t) \tau_m(t) dt = \frac{1}{2} \hat{\tau}^\top \beta_m I_N \hat{\tau} \quad (31)$$

where β_m is a penalty weight associated with the control-torque magnitude and I_N is the identity matrix of size N . Because the time-averaged power in the objective function, written in Eqn. (28), does not include the PTO efficiency, the penalty weight placed on the PTO torque is expected to act as a tuning parameter to tell the optimizer the PTO is less efficient. Positive results were observed in [9].

C. Final Objective Function

The objective function will be the sum of the time-averaged absorbed power, the squared ℓ^2 -norm of the surge-restraining force, and control-force magnitude. The three contributions to the objective function are not of the same units, and the interrelationship among them is complex. Therefore, the final objective function will consist of the following nondimensional quantities

$$J = \underbrace{\frac{P_T}{wP_w}}_{C_w} + \gamma \left| \frac{f_{r1}}{\frac{1}{2}\rho g w h A} \right|^2 + \beta_m \left| \frac{\tau_m}{\frac{1}{8}\rho g w h^2 A} \right|^2 \quad (32)$$

V. REGULAR WAVE RESULTS

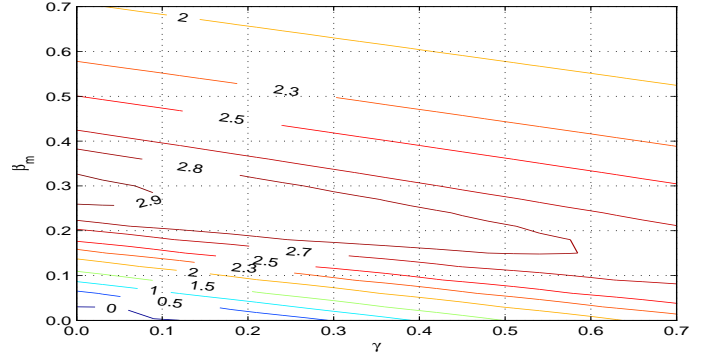
The pseudo-spectral control simulations were performed in regular waves with varying period and amplitude. The authors chose to use a mechanical-to-electrical conversion efficiency, η_e , of 80% and limited the WEC angular displacement amplitude to $30^\circ(\pi/6)$. As this work is focused on balancing power absorption against structural loads, the following power-to-load ratio, P_{tL} , was developed to evaluate the WEC performance

$$P_{tL} = C_w \left(\frac{C_w}{f_{r1}^* + \tau_m^*} \right) \left(\frac{P_O}{\sigma_O} \right) \quad (33)$$

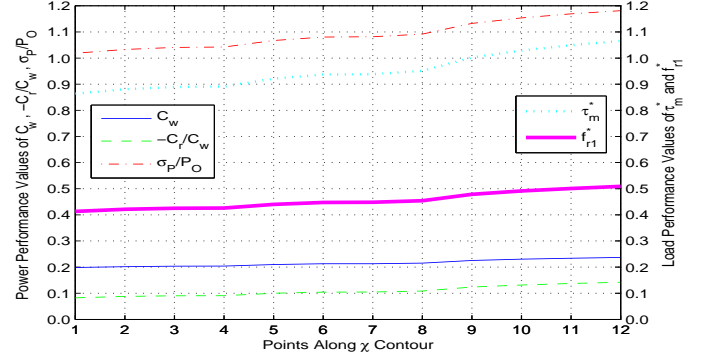
$$\chi = \frac{P_{tL}}{P_{tL}^{\eta_e}} \quad (34)$$

where σ_O is the standard deviation in the instantaneous output power. As this section considers regular waves, in the calculation of P_{tL} the values of f_{r1} and τ_m are taken as the peak values over the wave period. The first term in Eqn. (33) represents the net output power to the grid that is directly related to the characteristic drivers of economics; however, the second term is included to temper the controller from allowing large structural loads, leading to greater steel thickness and higher capital costs. The third term was introduced to limit the PTO peak instantaneous power and control actuation effort, thereby minimizing the PTO power-capacity requirements. The resulting P_{tL} ratios from applying PSC for various combinations of γ and β_m are compared against results from a baseline control case. The baseline control case will consist of solving for the coefficient pair of C_g and $\lambda_g \geq 0$ that maximizes the PTO output power and will be denoted by the superscript η_e .

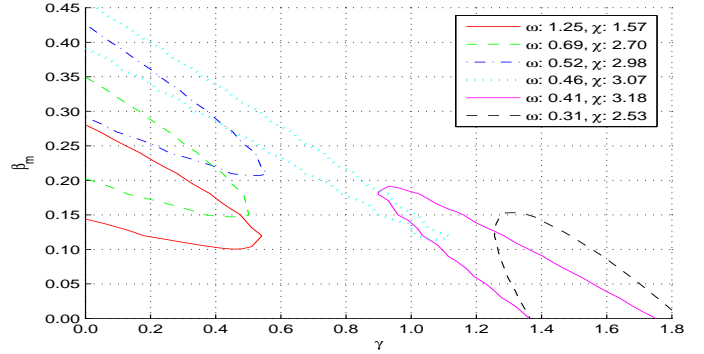
The χ ratio, given by Eqn. (34), has been plotted along constant contours in Fig. 9(a). The bottom left of the plot is where the greatest absorbed power can be achieved; however, the efficiency losses, greater structural loads, and peaks in instantaneous power decrease the benefit of operating the OSWEC in this penalty-weight region. Rather, there is a region where χ is maximized before decreasing as larger penalty weights place greater emphasis on load reduction at the cost of power absorption. Along the maximum χ contours, the individual performance metrics will vary as shown in Fig. 9(b). Although the output power has a maximum along the χ contour, it is followed by a proportionate growth in structural



(a) χ Contours for a Wave Amplitude of 0.25 m and Period of 10 s



(b) Performance Values Along the $\chi = 2.9$ Contour Shown in Fig. 9(a)



(c) χ Contours Across Multiple Wave Frequencies with an Amplitude of 0.25 m

Fig. 9. Results for the two-flap open geometry with a PTO efficiency of 80% in regular waves.

loads, peak instantaneous power, or a combination of the two. The range of penalty weights that provides the greatest χ values will vary depending on wave frequency as shown in Fig. 9(c); however, the optimum χ values can be susceptible to the nondimensionalization of loads as defined in Eqn. (32).

A. Performance Metrics from Greatest Power-to-Load Ratios

The first series of tests completed were for a fixed wave amplitude of 0.25 m while varying the wave period between 5 s and 20 s; the results are shown in the left column of Fig. 10 and Fig. 11. To compare results across wave frequencies, the maximum χ contours were calculated such that the enclosed

areas were the same size but may differ in location in the γ and β_m domain as shown in Fig. 9(c). The performance metrics along this χ contour were averaged for each frequency and plotted in Fig. 10. The results plotted in Fig. 10(a), show that PSC can be used to maximize the power-to-load ratio and exceed the baseline control case for any flap configuration. The zero-flap configuration provides the greatest power-to-load ratios with a step-like reduction as each additional flap is opened. The three-flap open configuration improves the P_{tL} near the associated resonance frequency; however, this is quickly lost as the wave amplitude increases and the pitch displacement constraint is observed.

It is evident that maximizing the power-to-load ratio does not coincide with maximizing the PTO output power (see Fig. 10(c)). When considering the zero-flap configuration, the average reduction in capture width between PSC and the baseline control strategy is near 37%, whereas the reduction in reactive power requirement is slightly more than 90%. Limiting the reactive power requirement also leads to significant reductions in the PTO control torque, Fig. 10(e), and surge-foundation force, Fig. 10(g). The zero-flap configuration achieves a 57% reduction in both load metrics when operating at the greatest power-to-load ratio. However, this reduction is only obtained when allowing for reactive power, providing greater control over the phase of the pitch-angular displacement [6]. These contributions allow PSC to provide the greatest P_{tL} for all wave frequencies while providing a moderate increase in power capture relative to passive control ($\lambda_g \geq 0$, $C_g = 0$), which is generally considered the current standard in the wave energy community.

Another series of tests were completed for a fixed-wave amplitude of 1.0 m to understand the effects of the pitch-motion constraint on controller performance and the results shown in the right column of Fig. 10 and Fig. 11. Similar trends are observed in the power-to-load ratio as the zero-flap configuration still provides the maximum values, but there is a local peak in the low-frequency regime (see Fig. 10(b)). This is a result of the OSWEC motion hitting the pitch-displacement constraint, Fig. 11(d), which prevented the optimum oscillation amplitude from being reached. As discussed at the end of Section III-A1, the baseline control case will be required to increase the PTO damping coefficient to meet the motion constraints. This reduces the motoring requirement of the PTO unit, which is followed by a decrease in structural loads per unit wave amplitude (see Fig. 10(f) and Fig. 10(h)).

VI. CONCLUSION

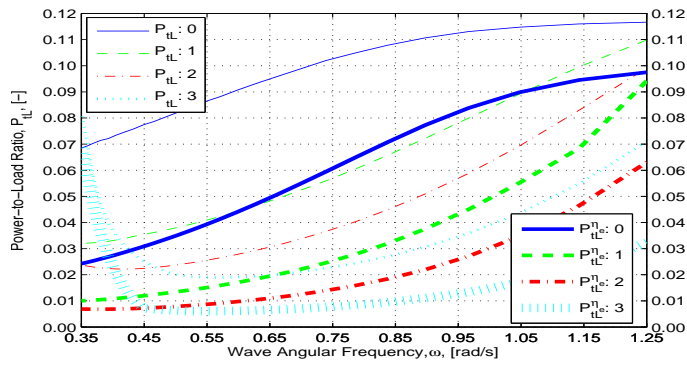
This paper has utilized pseudo-spectral control (PSC) with a multiterm objective function to balance power absorption against structural loading for a novel oscillating surge wave energy converter (OSWEC). The results from PSC were corrected to account for the losses associated with bidirectional energy flow when utilizing a nonideal power-take-off (PTO) unit. PSC performance was tuned based on the selected penalty weights, which allow controller emphasis to be placed on either power absorption or load mitigation. Although the PTO

efficiency was not directly represented in the objective function, the choice of certain penalty weight combinations leads the optimizer to converge toward the baseline control case while reducing the influence of the PTO efficiency on power absorption. Thus, future controller design may utilize penalty weights in the objective function to successfully represent losses associated with use of a nonideal PTO. This allows the objective function to remain convex, thereby reducing the computational demand and solution time. It was found that for certain penalty weight combinations, the surge-foundation force and PTO control torque magnitude decreased at a greater rate than output power, providing the greatest power-to-load ratios. However, the location of the optimum penalty weight contours varied based on the wave angular frequency and OSWEC geometry.

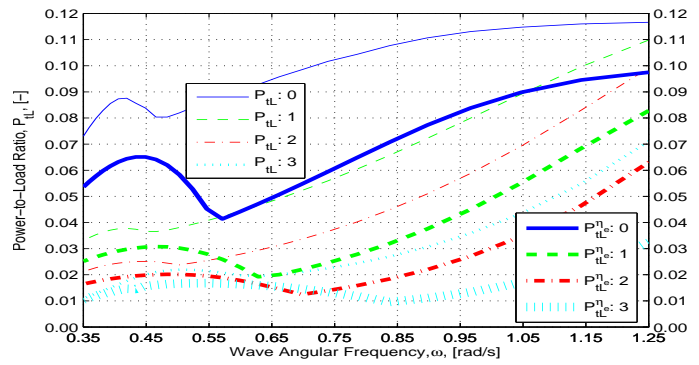
Although PSC has been used in previous investigations [6] and [30], this work has examined how reversing the order in which the flaps are opened affects the power and load performance. By opening the flaps from the bottom to top in ascending order, the reduction in the hydrodynamic coefficients was found not to be as large when compared to the descending top-to-bottom order [4]. However, the reductions in the hydrodynamic coefficients are still nonuniform and finer control may be obtained by utilizing a greater number of flaps with varying height [19]. This work has also shown that for a fixed-bottom OSWEC, the hydrodynamics favor the closed flap configurations when considering passive energy harvesting ($C_g = 0$). Therefore, the variable geometry will be predominantly for load shedding in moderate-to-large sea states while maintaining a rated power level. In moderate-to-large sea states the pitch-displacement constraint limits the adverse effects from a nonideal PTO. As the wave amplitude increased, the PTO damping coefficient must be increased to stay under the pitch motion constraint, thereby reducing the PTO spring-to-damping ratio. This convergence helps to explain why results from PSC at larger wave amplitudes have an increase in response after running into the pitch displacement constraint. Once the pitch displacement amplitude is limited, the PSC has fewer options in which to limit the structural loading, and the increases in the power-to-load ratio are reduced. The results from this work continue to demonstrate how shedding a portion of the available wave energy at any wave amplitude can lead to greater reductions in structural loading and reactive power requirement, which may assist in the realization of advanced control strategies.

ACKNOWLEDGMENT

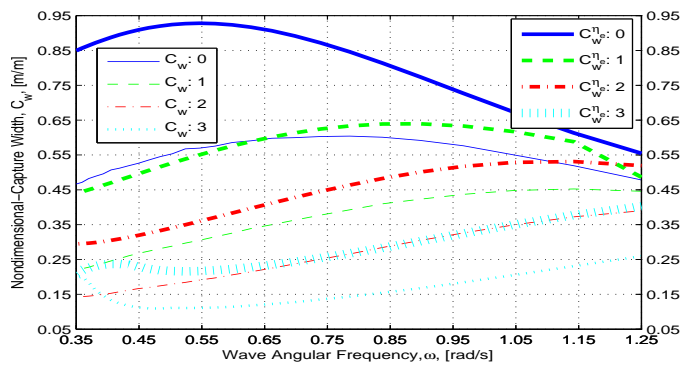
This work was supported by the U.S. Department of Energy under Contract No. DE-AC36-08GO28308 with the National Renewable Energy Laboratory (NREL). Funding for the work was provided by NREL's Laboratory Directed Research and Development Program. The U.S. Government retains and the publisher, by accepting the article for publication, acknowledges that the U.S. Government retains a nonexclusive, paid-up, irrevocable, worldwide license to publish or reproduce the



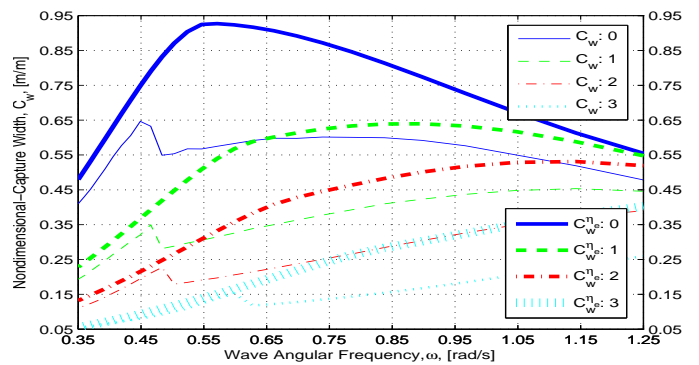
(a) Power-to-Load Ratio, P_{tL} , with a 0.25-m Wave Amplitude



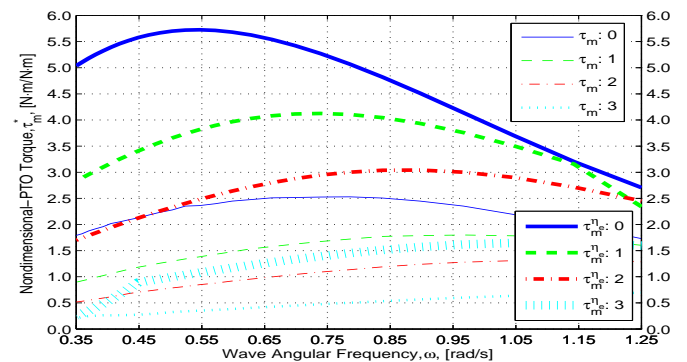
(b) Power-to-Load Ratio, P_{tL} , with a 1.00-m Wave Amplitude



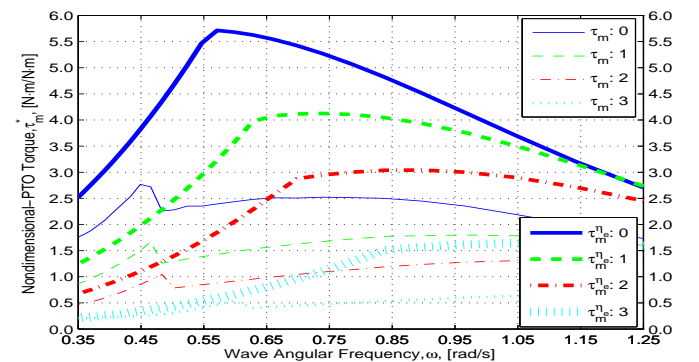
(c) Nondimensional-Capture Width, C_w , with a 0.25-m Wave Amplitude



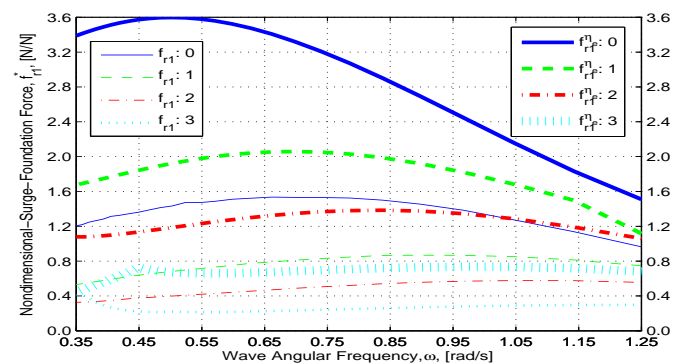
(d) Nondimensional-Capture Width, C_w , with a 1.00-m Wave Amplitude



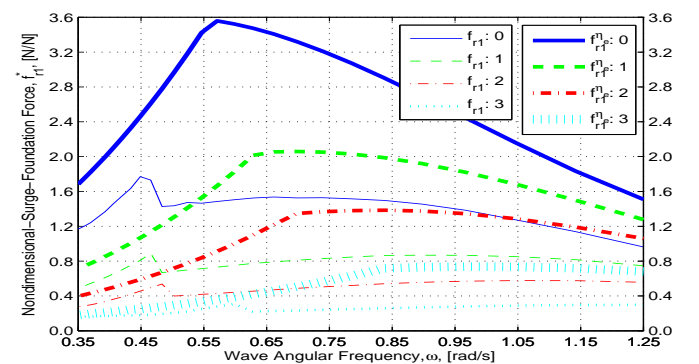
(e) PTO-Control Torque, τ_m^* , with a 0.25-m Wave Amplitude



(f) PTO-Control Torque, τ_m^* , with a 1.00-m Wave Amplitude



(g) Surge-Foundation Force, f_{r1}^* , with a 0.25-m Wave Amplitude



(h) Surge-Foundation Force, f_{r1}^* , with a 1.00-m Wave Amplitude

Fig. 10. The results for the power-to-load ratio, nondimensional-capture width, PTO-control torque, and surge-foundation force for the zero-, one-, two-, and three-flap open geometry with a PTO efficiency of 80%.

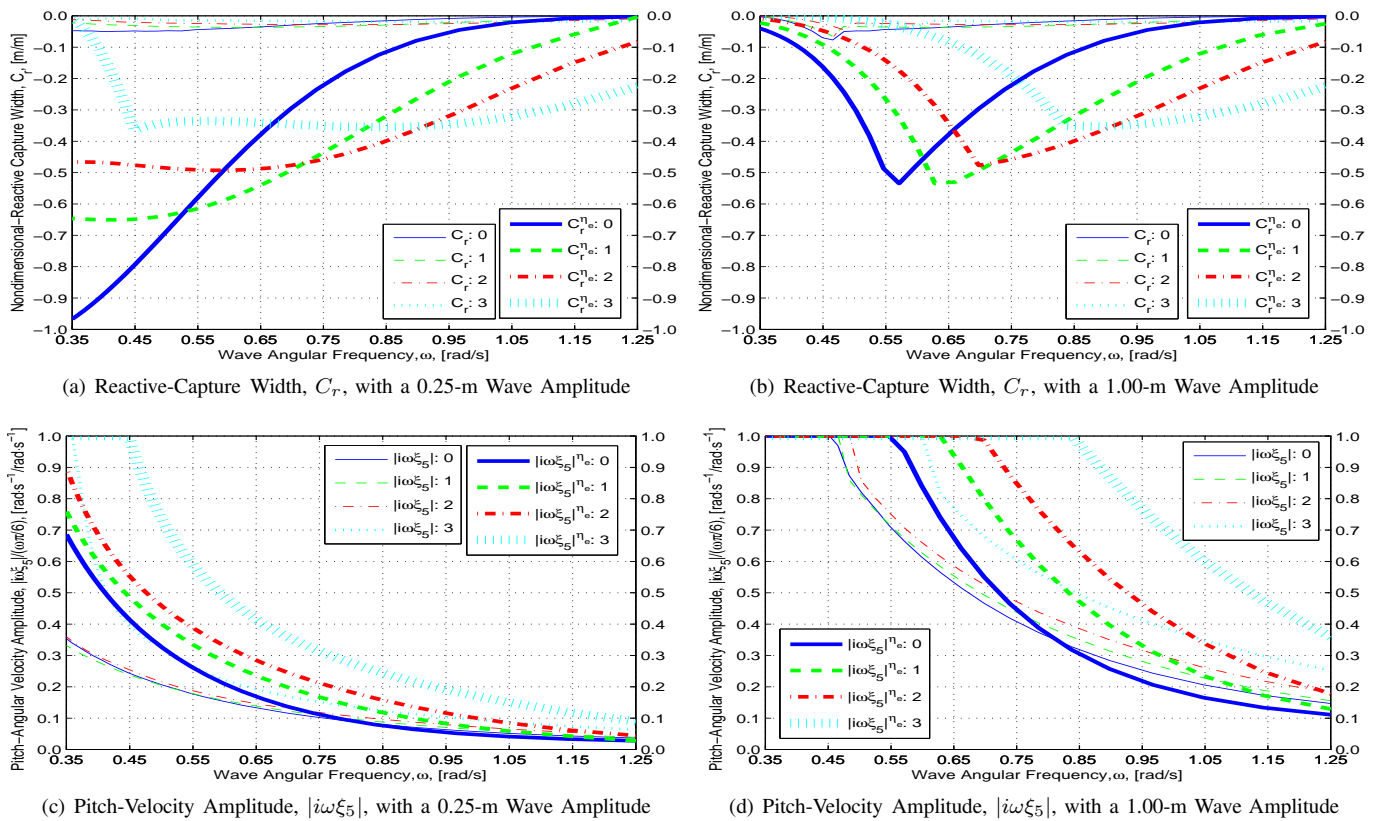


Fig. 11. The reactive power requirement and pitch displacement amplitude results for the zero-, one-, two-, and three-flap open geometry with a PTO efficiency of 80%.

published form of this work, or allow others to do so, for U.S. Government purposes.

REFERENCES

- [1] T. Whittaker and M. Folley, "Nearshore oscillating wave surge converters and the development of Oyster," *Philosophical Transactions Royal Society A*, vol. 370, pp. 345–364, 2012.
- [2] J. Lucas, M. Livingstone, M. Vuorinen, and J. Cruz, "Development of a wave energy converter (WEC) design tool-application to the WaveRoller WEC including validation of numerical estimates," in *Fourth International Conference on Ocean Energy*, Dublin, Ireland, 2012.
- [3] N. Tom, M. J. Lawson, Y.-H. Yu, and A. D. Wright, "Preliminary analysis of an oscillating surge wave energy converter with controlled geometry," in *Eleventh European Wave and Tidal Energy Conference*, Nantes, France, 2015.
- [4] N. Tom, M. J. Lawson, Y.-H. Yu, and A. D. Wright, "Spectral modeling of an oscillating surge wave energy converter with control surfaces," *Applied Ocean Research*, vol. 56, pp. 143–156, 2016a.
- [5] N. Tom, M. J. Lawson, Y.-H. Yu, and A. D. Wright, "Development of a nearshore oscillating surge wave energy converter with variable geometry," *Renewable Energy*, vol. 96, pp. 410–424, 2016b.
- [6] N. Tom, Y.-H. Yu, A. D. Wright, and M. J. Lawson, "Balancing power absorption and fatigue loads in irregular waves for an oscillating surge wave energy converter," in *35th International Conference on Ocean, Offshore, and Arctic Engineering*, Busan, South Korea, 2016c.
- [7] J. Falnes, "Optimum control of oscillation of wave-energy converters," *International Journal of Offshore and Polar Engineering*, vol. 12, no. 2, pp. 147–154, 2002.
- [8] A. Babarit and A. H. Clément, "Optimal latching control of a wave energy device in regular and irregular waves," *Applied Ocean Research*, vol. 28, pp. 77–91, 2006.
- [9] J. A. M. Cretel, G. Lightbody, G. P. Thomas, and A. W. Lewis, "Maximisation of energy capture by a wave-energy point absorber using model predictive control," in *18th World Congress of the International Federation of Automatic Control*, Milano, Italy, 2011.
- [10] N. Tom, F. Madhi, and R. W. Yeung, "Balancing power absorption and structural loading for an asymmetric heave wave-energy converter in regular waves," in *35th International Conference on Ocean, Offshore, and Arctic Engineering*, Busan, South Korea, 2016d.
- [11] A. S. Zurkinden, S. H. Lambertsen, L. Damkilde, Z. Gao, and T. Moan, "Fatigue analysis of a wave energy converter taking into account different control strategies," in *32nd International Conference on Ocean, Offshore, and Arctic Engineering*, Nantes, France, 2013.
- [12] H. Eidsmoen, "Optimum control of a floating wave-energy converter with restricted amplitude," *Journal of Offshore Mechanics and Arctic Engineering*, vol. 118, no. 2, pp. 96–102, 1996.
- [13] J. Hals, J. Falnes, and T. Moan, "Constrained optimal control of a heaving buoy wave-energy converter," *Journal of Offshore Mechanics and Arctic Engineering*, vol. 133, no. 1, 2011.
- [14] G. Bacelli and J. V. Ringwood, "A Control System for a Self-reacting Point Absorber Wave Energy Converter Subject to Constraints," in *18th World Congress of the International Federation of Automatic Control*, Milano, Italy, 2011.
- [15] D. R. Herber and J. T. Allison, "Wave energy extraction maximization in irregular ocean waves using pseudospectral methods," *International Design Engineering Technical Conferences and Computers and Information in Engineering Conference*, Portland, Oregon, USA, 2013.
- [16] G. Bacelli, R. Genest, and J. V. Ringwood, "Nonlinear control of flap-type wave energy converter with non-ideal power take-off system," *Annual Reviews in Control*, vol. 40, pp. 116–126, 2015a.
- [17] P. Tona, H. N. Nguyen, G. Sabiron, and Y. Creff, "An efficiency-aware model predictive control strategy for a heaving buoy wave energy converter," in *11th European Wave and Tidal Energy Conference*, Nantes, France, 2015.
- [18] WAMIT Version 7.2 User Manual, <http://www.wamit.com>, 2016.

- [19] M. Kelly, N. Tom, Y.-H. Yu, and R. Thresher, "Development of the second-generation oscillating surge wave energy converter with variable geometry," in *27th International Ocean and Polar Engineering Conference*, San Francisco, CA, USA, 2017.
- [20] R. P. F. Gomes, M. F. P. Lopes, J. C. C. Henriques, L. M. C. Gato, and A. F. O. Falcão, "The dynamics and power extraction of bottom-hinged plate wave energy converters in regular and irregular waves," *Ocean Engineering*, vol. 96, pp. 86–99, 2015.
- [21] D. V. Evans, "A theory for wave-power absorption by oscillating bodies," *Journal of Fluid Mechanics*, vol. 7, no. 1, pp. 1–25, 1976.
- [22] J. N. Newman, "The exciting forces on fixed bodies in waves," *Journal of Ship Research*, vol. 6, no. 3, pp. 10–17, 1962.
- [23] M. Folley, H. Henry, and T. Whittaker, "Contrasting the hydrodynamics of heaving and surging wave energy converters," in *11th European Wave and Tidal Energy Conference*, Nantes, France, 2015.
- [24] J. Hals, T. Bjarte-Larsson, J. Falnes, "Optimum reactive control and control by latching of a wave-absorbing semisubmerged heaving sphere," in *21st International Conference on Offshore Mechanics and Arctic Engineering*, Oslo, Norway, pp. 415–423, 2002.
- [25] D. V. Evans, "Maximum wave-power absorption under motion constraints," *Applied Ocean Research*, vol. 3, no. 4, pp. 200–203, 1981.
- [26] R. Genest, F. Bonnefoy, A. H. Clément, and A. Babarit, "Effect of non-ideal power take-off on the energy absorption of a reactively controlled one degree of freedom wave energy converter," *Applied Ocean Research*, vol. 48, pp. 236–243, 2014.
- [27] A. F. O. Falcao and J. C. C. Henriques, "Effect of non-ideal power take-off efficiency on performance of single- and two-body reactively controlled wave energy converters," *Journal of Ocean Engineering and Marine Energy*, vol. 1, no. 3, 273–286, 2015.
- [28] A. Kurniawan and T. Moan, "Characteristics of a pitching wave absorber with rotatable flap," *Energy Procedia*, vol. 20, pp. 134–147, 2012.
- [29] G. Bacelli and J. V. Ringwood, "Numerical Optimal Control of Wave Energy Converters," *IEEE Transactions on Sustainable Energy*, vol. 6, no. 2, pp. 133–145, 2015b.
- [30] N. Tom, Y.-H. Yu, M. J. Lawson, and A. D. Wright, "Pseudo-spectral control of a novel oscillating surge wave energy converter in regular waves for power optimization including load shedding," *Ocean Engineering*, 2017 (accepted for publication).